

Monitoring and spatio-temporal analysis of UHI effect for Mansa district of Punjab, India

Rajveer Kaur and Puneeta Pandey*

*Department of Environmental Sciences and Technology,
Central University of Punjab, Bathinda, Punjab-151001, India*

(Received November 15, 2019, Revised March 14, 2020, Accepted March 17, 2020)

Abstract. Urban heat island (UHI) is one of the most important climatic implications of urbanization and thus a matter of key concern for environmentalists of the world in the twenty-first century. The relationship between climate and urbanization has been better understood with the introduction of thermal remote sensing. So, this study is an attempt to understand the influence of urbanization on local temperature for a small developing city. The study focuses on the investigation of intensity of atmospheric and surface urban heat island for a small urbanizing district of Punjab, India. Landsat 8 OLI/TIRS satellite data and field observations were used to examine the spatial pattern of surface and atmospheric UHI effect respectively, for the month of April, 2018. The satellite data has been used to cover the larger geographical area while field observations were taken for simultaneous and daily temperature measurements for different land use types. The significant influence of land use/land cover (LULC) patterns on UHI effect was analyzed using normalized built-up and vegetation indices (NDBI, NDVI) that were derived from remote sensing satellite data. The statistical analysis carried out for land surface temperature (LST) and LULC indicators displayed negative correlation for LST and NDVI while NDBI and LST exhibited positive correlation depicting attenuation in UHI effect by abundant vegetation. The comparison of remote sensing and in-situ observations were also carried out in the study. The research concluded in finding both nocturnal and daytime UHI effect based on diurnal air temperature observations. The study recommends the urgent need to explore and impose effective UHI mitigation measures for the sustainable urban growth.

Keywords: urban heat island (UHI); land surface temperature; remote sensing; NDVI; NDBI

1. Introduction

With the ongoing development in the era of urbanization, more than half of the world's population (~54%) has been reported to reside in urban areas in the year 2014 and is expected to rise up to 66% by 2050 (United Nations 2014). The swift urban population growth has altered land use land cover (LULC) patterns throughout the world by conversion of vegetation and green cover into dense urban infrastructure and built-up areas that have consequently expanded the urban clusters (Vitousek *et al.* 1997). So, the significant variations in thermal conditions of these expanded urban areas are the direct implication of change in LULC induced by urbanization; that

*Corresponding author, Assistant Professor, E-mail: puneetapandey@gmail.com

thus causes urban-rural temperature contrast, which is popularly known as 'Urban Heat Island' (UHI) (Oke 1982, Chakraborty *et al.* 2015). UHI is a major environmental issue related to urban climate, the concept of which was introduced by Luke Howard in 1833. The UHI hence, can be elaborated as the phenomenon of higher temperature of urban areas than surrounding suburban and rural areas (Oke 1982).

The urban areas with impervious surfaces and dense infrastructure have low sky-view factor, evapo-transpiration rates, and soil moisture than rural areas (Oke 1981, Svensson 2004). Additionally, the urban clusters due to different thermal characteristics such as high heat storage capacity, thermal emissivity and low solar reflectance; possess higher sensible heat flux from land surfaces while higher latent heat flux is observed in rural areas with higher vegetated surfaces and water bodies (Gallo *et al.* 1993, Taha 1997, Mohan *et al.* 2012). This increase in sensible heat flux by various urban surfaces causes urban-rural temperature difference, or in other words, the UHI effect.

The intensity of UHI phenomenon depends on the extent of urbanization, topography, urban geometry, surface characteristics, density of built-up area, solar insolation, anthropogenic heat, vegetated areas and meteorological conditions (Oke 1987, Taha 1997, Sun *et al.* 2010). The variations in UHI effect also depends on the day and night-time air circulations. The heat island effect is more frequent for calm atmospheric conditions especially at night-time for clear sky (Kim and Baik 2004, Lam *et al.* 2005).

The UHI effect, been reported in even small urban areas having population less than 10,000 (Karl *et al.* 1988), is known to degrade urban environment quality. So, this phenomenon has numerous environmental implications such as it increases air pollution (Sarrat *et al.* 2006, Han *et al.* 2009), changes water quality (Gober *et al.* 2009), alters precipitation patterns (Grimm *et al.* 2008, Shastri *et al.* 2015) and increases energy requirement (Santamouris *et al.* 2015). The UHI phenomenon is also known to affect human health (Lo and Quattrochi 2003, Kovats and Hajat 2008) due to the higher temperature and thermal discomfort (Steenefeld *et al.* 2011).

Based on the method of measurement, the UHI phenomenon is characterized as atmospheric and surface UHI phenomenon. Surface UHI is the phenomenon of the temperature difference between urban and rural land surfaces while atmospheric UHI is associated with the air temperature of urban and rural canopies (Yuan and Bauer 2007). Meanwhile, numerous studies have contributed towards this thermal phenomenon by estimating air temperature either through the conventional method of field measurements, mobile transitory pathways or from weather stations for analysis of atmospheric UHIs (Landsberg 1981, Eliasson 1994). As a recent alternative approach of ground-based measurements, the spatio-temporal patterns of LST can be readily retrieved with the introduction of thermal remote sensing combined with Geographical Information System (GIS) technique for surface UHI effect estimation (Imhoff *et al.* 2010). A variety of sensors with different spatial and spectral resolution are nowadays available that includes National Oceanic and Atmospheric Administration-Advanced Very High Resolution Radiometer (NOAA -AVHRR) (Roth *et al.* 1989, Streutker 2002), Advanced Space-borne Thermal Emission and Reflection (ASTER) (Liu and Zhang 2011), Moderate Resolution Imaging Spectro-radiometer (MODIS) (Rajasekar and Weng 2009, Pandey *et al.* 2012), Landsat TM/ETM+ (Chen *et al.* 2006, Klok *et al.* 2012). Besides, the Landsat program has been significantly contributing in Earth surface monitoring studies since the launch of its first satellite in 1972 (Phiri and Morgenroth 2017). So, these enduring advancements in resolution of satellite data have significantly contributed for research regarding UHI effect throughout the world (Liu and Zhang 2011). The remote sensing technology can also be used to estimate vegetation indices, surface

parameters like temperature, emissivity and albedo that are significant in UHI studies.

The existing literature shows the occurrence of UHI been documented throughout the urban areas of world such as in Seoul (Kim and Baik 2005), London (Kolokotroni and Giridharan 2008), USA (Rajasekar and Weng 2009), Netherlands (Klok *et al.* 2012), China (Zhang *et al.* 2013). According to estimation, UHI effect has been reported in more than 1100 cities worldwide, irrespective of climatic conditions, size of the urban area, its latitude, scale and altitude (Stewart 2011).

The estimation of air and land surface temperature had remained a major focus for most of the UHI studies. The UHI indicators such as NDVI, percent impervious area, NDBI etc has also been widely studied to estimate LULC impact on UHI. In this context, a number of studies have been carried out such as the influence of urban LULC on temperature has been studied by Gallo *et al.* (1993) using surface temperature and NDVI. Yuan and Bauer (2007) investigated relationship between surface UHI indicators i.e., LST, NDVI and percent impervious surface area for the Metropolitan area of Minnesota using Landsat satellite data. Temporal analysis of NDVI and LST was carried out using NOAA-AVHRR satellite data by Julien *et al.* (2011). Li *et al.* (2014) analyzed the relationship between LST and land use type for Shanghai, China concluding that beyond the type of land cover, anthropogenic forces also affect urban UHI. Other than analyzing UHI effect, the influence of meteorological parameters such as speed and direction of wind and cloud cover on the intensity of UHI effect has been determined for New York City by Gedzelman *et al.* (2003). The urban characteristics such as size and shape of the urban area and its composition were analyzed as driving factors of UHI intensity for Paris (Lemonsu *et al.* 2015). The effect of surface geometry on satellite retrieved LST was estimated by Voogt and Oke (1998).

The Indian sub-continent facing one of the highest population growths with 377 million of urban population also not lags behind in analyzing the UHI effect. But the studies in developing country like India are limited only to a few metropolitan or mega-cities due to the size of remaining cities and density of the population in these cities. Some of the previous UHI studies conducted in India are mentioned here. Kikon *et al.* (2016) estimated the UHI effect using multi-temporal satellite data for Noida, India. The study showed an increase in temperature with increase in impervious area for the year 2000 and 2013. The researchers also conducted a statistical analysis between UHI and albedo, NDBI, NDVI and emissivity, to find out the correlation among LST and LULC. Shastri *et al.* (2017) made an attempt to investigate surface UHI effect for diurnal and seasonal characteristics for 84 locations in urban and surrounding rural areas of India, using MODIS data. Mukherjee *et al.* (2017) carried out a study for 12 districts of Punjab, India using downscaled MODIS data. The Landsat TM satellite data was explored for urban area of Delhi to estimate seasonal variations in UHI effect by Singh *et al.* (2014). Similarly, the impact of change in LULC from 1999 to 2006 on LST was studied by Nesarikar-Patki and Raykar-Alange (2012) for Pune, India. The study concluded in finding an increase of 1-4°C in LST with 32.48% increase in built-up area and a certain decrease in area under vegetation and barren land. Borbora and Das (2014) carried out another UHI study for summer months for Guwahati, India using in-situ temperature measurements. The spatio-temporal changes in UHI were studied for Delhi, India with respect to LULC variations (Pandey *et al.* 2014) in which urban-rural temperature contrast was also observed for different seasons as well as during day and nighttime.

Despite these few Indian UHI studies, very less number of studies have been conducted that involve both LST from remote sensing data and air temperature by field observations for UHI estimation. So, in context of this discussion, this paper focuses on the specific objectives: a) to compute the urban-rural air and surface temperature difference for UHI estimation for Mansa

district of Punjab, India, b) to investigate spatial distribution of LULC by using NDBI and NDVI indices, c) to compare air temperature recorded by field observations and LST derived from remote sensing data, d) to examine the correlation between LST and NDBI and NDVI.

2. Materials and methods

2.1 Study area

The Mansa district is located in Malwa region of southern Punjab that came into existence in 1992 from the former Bathinda district. It is known as cotton belt of Punjab. The study area as shown in Fig. 1 lies between 29°32': 30°12' N and 75°10': 75°46' E with total geographic area of 2174 sq km (<https://mansa.nic.in/>). The district is covered in topographic sheet 44 N/08,12 and 44 O/01,02,05,06,09. It is bordered by Sirsa district of Haryana in south, Sangrur district in east, Barnala district in north and Bathinda district in west. The Mansa district is categorized into three sub-divisions (Mansa, Budhlada and Sardulgarh) and five blocks (<http://mansa.nic.in/html/about.html>). About 27 sq km of district area is covered under forest area, 1900 sq km is net sown area and 139 sq km is permanent fallow land of district. As per population census 2011, total population of Punjab is 27,743,338 while total population of Mansa district is 769,751 out of which 163,604 is urban population and remaining 606,147 is rural population. The population density of district is 350 per sq km. There has been 11.76% decadal population growth in the district between the years 2001-2011.

The district faces typical semi-arid type climate which can be further categorized as sub-tropical steppe, semi-arid and hot. The district is generally dry except the monsoon season (June to September) receiving southwest monsoon with average annual rainfall of 378 mm. The months of July and August are recognized as rainiest months for the region. Besides, the district has extremely high temperature in summer (48°C-May, June) and low in winters (3.5°C-January) (PCA, 2011).

The table below (Table 1) represents the geographical co-ordinates of the study sites selected for air temperature estimation. The sites S1 and S2 mentioned in the table lie inside the core of the city encircled in Google Earth image (Fig. 2) while sites S3 and S4 are few meters apart from the urban cluster. The remaining two sites S5 and S6 are the rural sites surrounding the Mansa urban area. None of the UHI studies using ground measurements have been conducted till date for Mansa district of Punjab. Thus, this study is maiden attempt to report UHI occurrence using air temperature in this region.

Table 1 Geographical co-ordinates of the study sites for air temperature

Site code	Site name	Site description	Latitude	Longitude
S1	Near Cinema road	Urban	29.99289°	75.39954°
S2	Nangal colony	Urban	29.98148°	75.40744°
S3	Arvind Nagar	Urban	30.01298°	75.39224°
S4	Green valley colony	Urban	29.9791°	75.38123°
S5	Chakeriyan	Rural	29.97732°	75.45026°
S6	Barnala	Rural	29.94837°	75.43394°

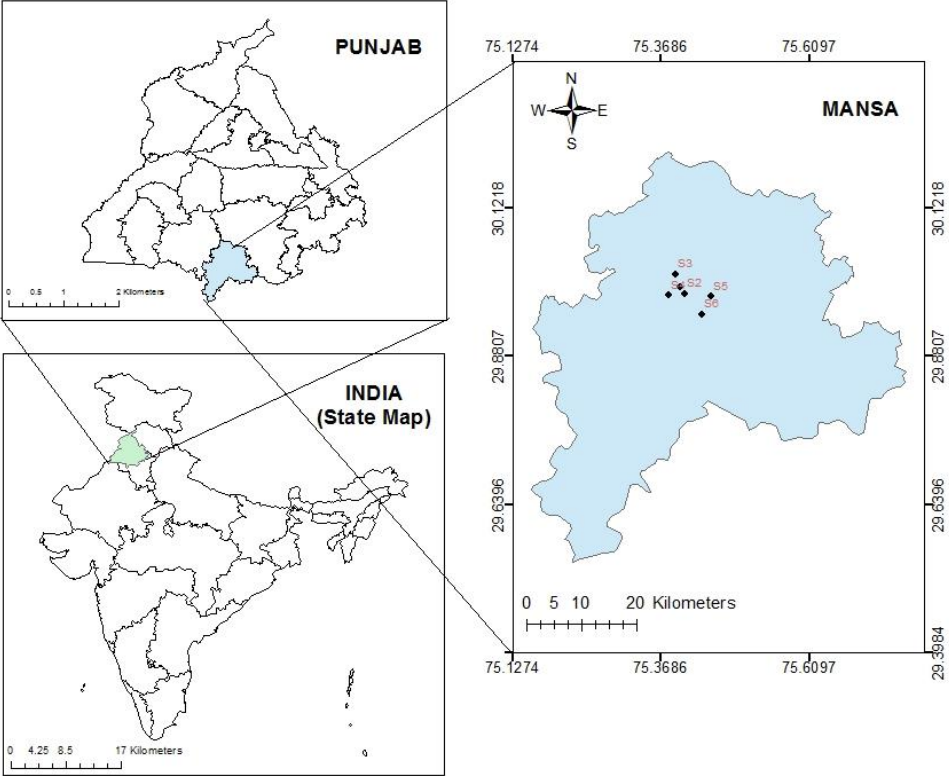


Fig. 1 Schematic diagram showing location map of study area

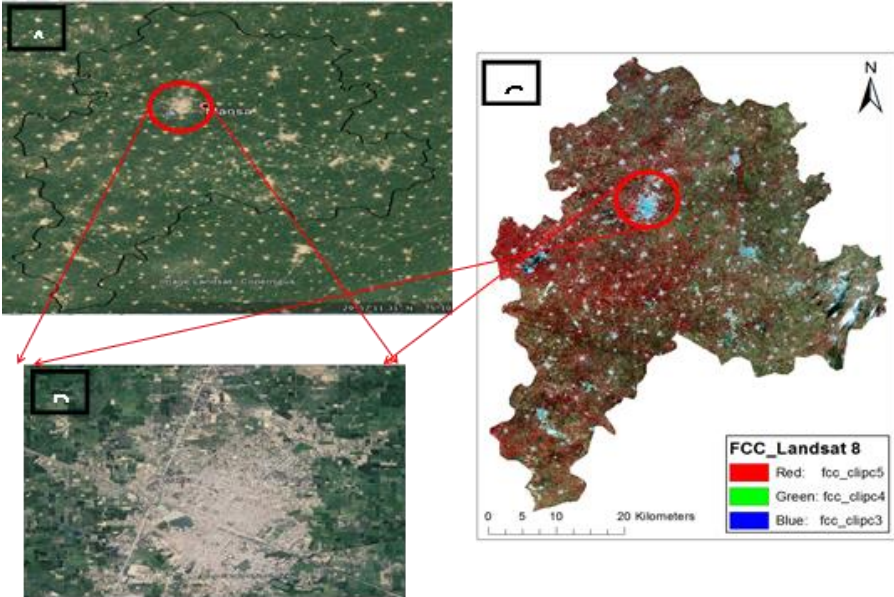


Fig. 2 Google Earth images of (a) boundary of Mansa district, (b) urban settlements of Mansa city and (c) False color composite image of Mansa district

Table 2 Specifications of satellite data used in this study

Satellite	Sensor	Path	Row	Image Acquisition Date	Spatial resolution	Temporal resolution	Spectral range
Landsat 8	OLI/TIRS	148	39	7 th April, 2018 23 rd April, 2018	30-100 m	16 days	0.43-12.51 μm

2.2 Data collection

2.2.1 Satellite data

The use of satellite data is getting wider due to its real time data analysis. The Landsat data has undergone several advancements in spatial and spectral resolution from Landsat 3 to Landsat 8, launched in the years 1978 and 2013, respectively (Markham *et al.* 2004). The two thermal bands of Landsat 8 (band 10 and 11) have application of retrieval of surface temperature values.

In this study, two Landsat 8-OLI/TIRS (Operational Land Imager/Thermal Infrared Sensor) images without cloud cover, with below tabulated (Table 2) specifications were procured from United States Geological Survey (USGS) Earth Explorer website for LST, NDVI and NDBI estimation of the study area. The satellite data was processed in ArcGIS 10.7 software for the current study.

2.2.2 Field data

In this study, due to the lack of official meteorological stations in the district, air temperature measurements were taken by placing thermometers at various residential buildings in the city and surrounding rural sites. The Mextech Digital thermometer with range from -50°C to $+200^{\circ}\text{C}$ has been used for daily air temperature measurements. The in-situ air temperature measurements were carried out at six sites at an interval of three hours for both the day and nighttime for the month of April, 2018. Out of the six sites selected for air temperature measurement, four sites lies inside and two outside the city representing surrounding rural area. Furthermore, Garmin GPS was used to note down the geographical co-ordinates of selected sites.

2.3 Methodology

The LST estimation was carried out using the following steps reviewed from literature and described in Landsat 8 Data Users Handbook:

Step 1: Conversion to Top of Atmospheric (TOA) Radiance-The thermal band of Landsat 8 OLI/TIRS data was first converted to TOA radiance using following equation:

$$L_{\lambda} = M_L Q_{\text{cal}} + A_L \quad (1)$$

where, L_{λ} = TOA radiance in $\text{W}/(\text{m}^2 \times \text{Sr} \times \mu\text{m})$, M_L = multiplicative rescaling factor, A_L = additive rescaling factor, Q_{cal} = quantized calibrated pixel value in digital number

Step 2: Conversion of TOA Radiance to Brightness Temperature (T_B)-The TOA radiance was then converted to Brightness Temperature (in $^{\circ}\text{C}$) using thermal band data of Landsat 8 OLI/TIRS as follows:

$$T_B = K_2 / \ln \left(\frac{K_1}{L_{\lambda} + 1} \right) - 273 \quad (2)$$

where, K_1 and K_2 are calibration constants (provided in metadata file)

Step 3: Estimation of Normalized difference vegetation index (NDVI)-NDVI is a vegetation index with its value lies between +1 and -1. The positive (higher) NDVI values represent higher extent of vegetation while the negative (lower) values indicate non-vegetative surfaces. The index is calculated by using unique spectral characteristics of green vegetation from the following equation (Dai *et al.* 2018):

$$NDVI = \frac{R_{NIR} - R_{Red}}{R_{NIR} + R_{Red}} \quad (3)$$

R_{NIR} = reflectance in near infrared band, Band 5 (0.85-0.88 μm) for Landsat 8

R_{Red} = reflectance in red band, Band 4 (0.64-0.67 μm) for Landsat 8

Step 4: Estimation of fractional vegetation cover (FVC)- The FVC estimation was done using minimum and maximum NDVI values (Stathopoulou *et al.* 2007).

$$FVC = \left(\frac{NDVI - NDVI_{min}}{NDVI_{max} - NDVI_{min}} \right)^2 \quad (4)$$

Step 5: Estimation of land surface emissivity (ϵ)- The land surface emissivity was derived from NDVI using the following equation (Sobrino *et al.* 2004, Rajeshwari and Mani 2014):

$$\epsilon = \epsilon_s(1 - FVC) + \epsilon_v \times FVC \quad (5)$$

Step 6: Estimation of Land surface temperature (T)-The land surface temperature is computed from Landsat 8 data using following equation of Mono-window algorithm (Artis and Carnahan 1982, Kumari *et al.* 2018):

$$T = \frac{T_B}{[1 + (\lambda T_B / c_2) \ln(\epsilon)]} \quad (6)$$

where, λ = wavelength of emitted radiance in μm , $c_2 = hc/s$ (h =Planck's constant, s =Boltzmann constant, c =velocity of light in m/s)

Estimation of Normalized difference vegetation index (NDBI): This index is significant for estimation of impervious built-up surfaces. The following equation was used for estimation of NDBI using Landsat 8 data (Zha *et al.* 2003, Habert *et al.* 2016):

$$NDBI = \frac{R_{SWIR} - R_{NIR}}{R_{SWIR} + R_{NIR}} \quad (7)$$

where, R_{SWIR} = reflectance in short wave infrared band, Band 6 of Landsat 8 (1.57-1.65 μm),

R_{NIR} = reflectance in near infrared band, Band 5 (0.85 – 0.88 μm) for Landsat 8

3. Results and discussion

3.1 Air temperature and atmospheric UHI

3.1.1 Air temperature variations

The significant variations in daily air temperature at an interval of three hours were observed for the month of April, 2018 for six different sites of the Mansa district as shown in Figs. 3 and 4 for the day and nighttime, respectively. Amongst all the days of the field campaign, the highest

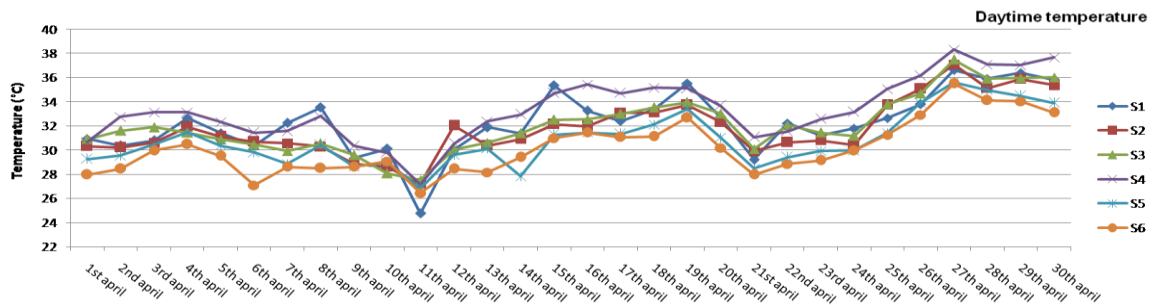


Fig. 3 Air temperatures for six selected sites from 1st April to 30th April, 2018 for both day and nighttime

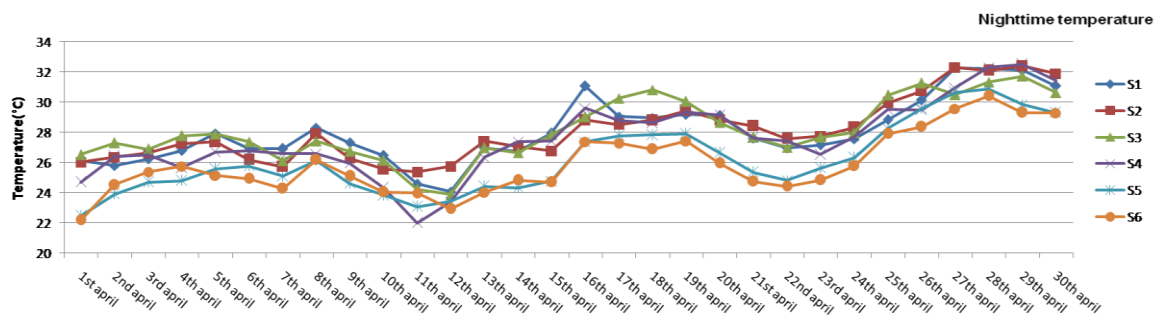


Fig. 4 Air temperatures for six selected sites from 1st April to 30th April, 2018 for both day and nighttime

ambient air temperature was recorded on 28th April, 2018 i.e., 40.8°C for urban site (S4) while lowest temperature of 18.9°C was observed near green areas of rural sites (S6) on 1st April, 2018 except during the rainfall.

The in-situ measurements for air temperature depict the highest temperature for S4 and lowest temperature for S5 during the daytime whereas S3 and S5 have highest and lowest temperature during the nighttime for the overall study period. This shows the low temperature for rural sites with green cover. The site S1 and S2 being in the urban core shows average highest air temperature both during the day and nighttime. So, the variations in air temperature can be seen for different land cover types of the district. The evapo-transpiration due to vegetation causes drop in air temperature of the rural regions. Previous studies have reported the decrease in air temperature of about 1-5°C because of the evapo-transpiration by vegetated surfaces (EPA 2009, Farina 2012).

3.1.2 Atmospheric UHI effect

The three hourly urban-rural air temperature measurements were averaged and subtracted to compute magnitude of UHI effect. The average UHI of magnitude 1.80°C was observed at 12:00 am, 2.04°C at 3:00 am, 2.43°C at 6:00 am, 1.81°C at 9:00 am, 1.97°C at 12:00 pm, 1.98°C at 3:00 pm, 1.67°C at 6:00 pm and 1.48°C at 9:00 pm. So, the mean UHI intensity lies between 1.5°C to 2.5°C for day and nighttime. Also, the average UHI was highest for 6:00 am depicting that highest UHI effect occurs for the study area during early morning hours i.e., before the sunrise.

The maximum nocturnal UHI of magnitude 4.75°C was observed on 13th April at 6.00 am and maximum daytime UHI of magnitude 3.62°C was recorded for 14th April at 12.00 pm; during the

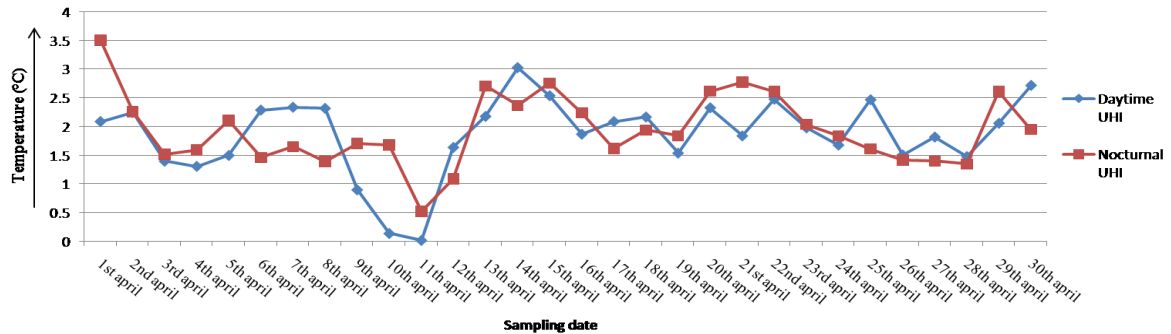


Fig. 5 The average UHI effect for day and nighttime for the April, 2018 for Mansa district

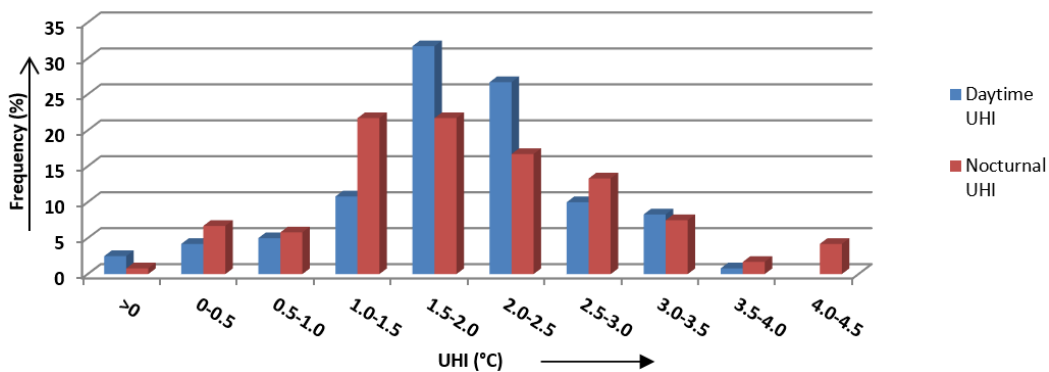


Fig. 6 Frequency of UHI of different magnitudes for day and nighttime

entire study period. The higher urban-rural temperature contrast has been reported during nighttime for previous studies also (Oke 1987, Azevedo *et al.* 2016). Fig. 5 shows the average UHI pattern for day and nighttime during the month of April 2018.

The dense urban infrastructure for urban sites (S1-S4) with residential buildings, commercial shops etc and low green cover have higher air temperature than surrounding rural regions. The busy traffic with certain emissions because of bus stand and railway station in the city clusters also builds up the heat island in the region. Moreover, the lower emission of long-wave radiation during the nighttime by urban surfaces traps the heat inside urban clusters consequently increasing urban temperature than surrounding rural areas.

The significant daytime UHI has been reported in previous studies carried out in Hong Kong by Giridharan *et al.* (2004), in Spain by Alonso *et al.* (2003). So, the results of this study are in consistence with earlier study conducted by Mohan *et al.* (2012) for Delhi, which reveals higher temperature of urban areas with dense infrastructure and also high UHI intensity for afternoon and night hours.

The frequency diagram (Fig. 6) shows that the UHI intensity of magnitude 1.5-2.0°C is most frequent for the region for both day and nighttime. However, higher intensity UHI (4.0-4.5°C) occurs only for the nighttime. Furthermore, the nocturnal UHI as can be seen from frequency diagram is more prominent for the Mansa district. This trend of nocturnal heat island is in conformity with the study done by Yuan and Bauer (2007) that states higher atmospheric UHI

effect for the nighttime.

Meanwhile, the decrease in urban temperature was observed due to rainfall on 9th, 10th and 11th April. This decrease in temperature nullified the UHI effect for respective days.

3.2 Spatial pattern of LST and surface UHI

The estimation of land surface temperature is a key step for UHI analysis as it is identified to affect UHI phenomenon the most (Liu and Zhang 2011). Two different dated (7th and 21st April, 2018) LST maps were prepared using Landsat 8 data for Mansa district as shown in Fig. 7(a) and 8(a). The map (7(a)) illustrates the land surface temperature variation from 38.46°C to 16.40°C with an average LST of 28.70°C for 7th April, 2018. The highest land surface temperature in the range of 38.46°C-30.95°C was observed for urban built-up areas with very low or no vegetation whereas the nearby rural areas with agricultural land exhibited comparatively low temperature. The water bodies located in the study area however have lowest temperature lying between 25.32°C-16.41°C.

The map (8(a)) illustrates the land surface temperature variation between 48.36°C and 27.91°C with an average LST of 41.25°C for 23rd April, 2018. The surface temperature difference of 10°C was noticeable between two images within the period of 16 days. This difference is due to the changing season i.e. winters to summer and more probably due to harvesting of wheat crops in agricultural fields of the study area. The loss of crops led to decreased green cover and hence increased temperature. The highest land surface temperature (41.23°C-48.36°C) for this image was observed for built-up areas and open surfaces without vegetation as well. The water bodies and trees/vegetation surrounding these water bodies have lowest temperature in the range (38.42°C-27.91°C) for 23rd April.

The visual analysis of the images demonstrates the spatial pattern of the LST. The map 7(a) shows higher temperature for eastern part of the district while temperature was more dispersed across the district for map 8(a). The results for LST over agricultural land are in accordance with study done by Chakraborty *et al.* (2015) for Delhi, India. The noticeable decrease in temperature while moving from the core of the city towards surrounding regions, is also in validation with the existing literature that states the proportion and density of vegetation and impermeable surfaces, as reason behind these temperature variations (Zhang *et al.* 2013, Adams and Smith 2014, Mallick 2014).

The urban-rural temperature contrast for the study area can be clearly seen from two images. The dense settlements occupying larger area showed higher temperature such as for Mansa city while small towns with low density residential areas have comparatively low temperature that was although higher than rural sites. The average temperature difference of approximately 4°C was observed between higher density settlements (34.7°C) and low density residential surfaces (30.03°C). Although, besides the density of buildings, the surface temperature also depends on multiple factors that include the thermal characteristics of the building surfaces, impervious surfaces made up of concrete, asphalt, vegetation cover, water bodies and LULC of area (Kuang *et al.* 2015). The sparse settlements of rural areas have lower temperature than dense urban buildings but higher than that of vegetated areas. Moreover, agricultural land covering most of rural pixels show temperature of 27.225°C while the water bodies of the region displayed lowest temperature (20.865°C). So, the decrease in temperature can be observed while moving from urban cores to the periphery of city and further drop in temperature occurs while moving away from the city i.e., towards rural areas. In other words, land surface temperature was found to show a decreasing

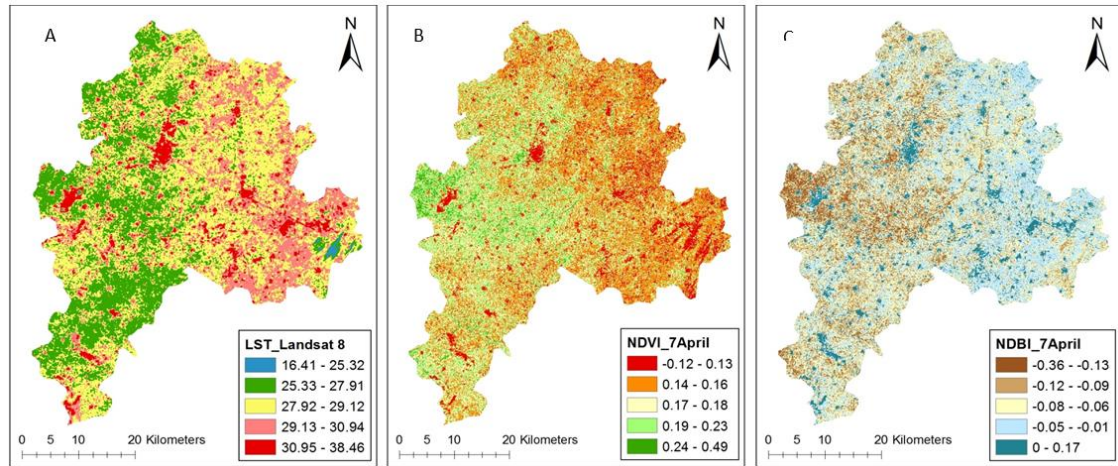


Fig. 7 Maps obtained for 7th April, 2018 using Landsat 8 OLI/TIRS images for (a) LST, (b) NDVI and (c) NDBI of Mansa district

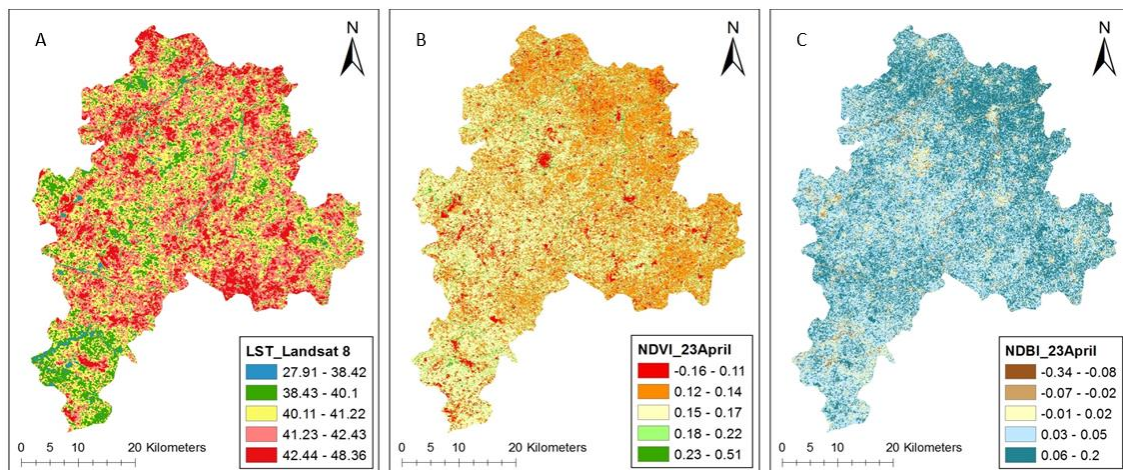


Fig. 8 Maps obtained for 23rd April, 2018 using Landsat 8 OLI/TIRS images for (a) LST, (b) NDVI and (c) NDBI of Mansa district

Table 3 UHI intensity of some major Indian cities reported in literature

Sr. no.	Study area	Climate	Study period	Data used	UHI intensity	Reference
1.	Four cities of Punjab, India	Sub-Tropical and semi-arid	September, 2010	MODIS data	Mean UHI: 6.4 °C	Mukherjee <i>et al.</i> (2017)
2.	Delhi, India	Humid sub-tropical climate	May 2008	Field observations	Daytime UHI: 3.8°C to 7.6°C Nighttime UHI: 2.8°C to 8.3°C	Mohan <i>et al.</i> (2012_)
3.	Delhi, India	Humid sub-tropical climate	January 2010 to December 2013	Field observations	Maximum UHI: 3°C Minimum UHI: 0.2°C	Yadav <i>et al.</i> (2017)

Table 3 Continued

Sr. no.	Study area	Climate	Study period	Data used	UHI intensity	Reference
4.	Guwahati, India	Humid sub-tropical climate	1May to 17 October 2009	Field observations	Maximum daytime UHI: 2.12°C Maximum nighttime UHI: 2.29°C	Borbora and Das (2014)
5.	Chandigarh, India	Humid sub-tropical climate	2009-2013	MODIS data	Average seasonal UHI: 3.84K to 6.16K	Mathew <i>et al.</i> (2016)

pattern for urban sites followed by semi-urban and rural sites confirming the formation of surface urban heat island of magnitude of 4-8°C for Mansa district.

Higher absorption of solar radiations by dense urban buildings, variations among thermal characteristics of urban-rural surfaces and reduced evapo-transpiration rates can be categorized as key factors accountable for UHI occurrence (Streutker 2002). The trends of the current study are consistent with some studies conducted in past such as higher temperature of dense built-up areas have been reported by Cheng *et al.* (2010), Mallick (2014), Mukherjee *et al.* (2017), Mathew *et al.* (2018) as shown in Table 3.

3.3 NDVI

The quantitative investigation of the vegetation for study area has been done by this vegetation index. Figs. 7(b) and 8(b) demonstrate the spatial pattern of NDVI for the study area. The highest NDVI value for the study area is 0.49 while -0.12 is the lowest NDVI value with an average of 0.16 for 7th April, 2018. The NDVI map suggests that the green areas are inclined more towards the western part of the district for 7th April, 2018 as high NDVI values ranging from 0.19 to 0.49 corresponding to vegetated surfaces such as agricultural fields, trees or plantation are visualized in this region of the district. The residential areas without vegetation have low NDVI values in the range of 0.13 to -0.12. The urban areas of Mansa district i.e., Mansa city and small towns present in the district with dense settlements show low NDVI values.

In the second image, for 23rd April, the highest NDVI value is 0.51 while lowest value is -0.16 with an average of 0.14. Although the maximum NDVI value is higher for 23rd April but there is decrease in average NDVI value for 23rd April due to crop harvesting and hence, there is a tremendous change in vegetation distribution.

The clear difference in vegetation patterns can be observed on comparison of NDVI values for urban and surrounding rural areas. The urban areas have low NDVI values due to low vegetation because of higher built-up surfaces in urban clusters while the rural areas have abundance of agricultural land with crops sown. The areas having higher NDVI value are represented with dark green color green areas whereas NDVI values below zero or near to zero are displayed by red color representing non-vegetated surfaces such as barren lands, built-up areas. So, the higher NDVI areas were mostly covered in rural regions corresponding to the agricultural lands. But with the harvesting of crops, this agricultural land appears as barren land resulting in higher LST.

Different evaluations have been made regarding NDVI values in literature. The urban-rural contrast for NDVI values has been evaluated because of the different surface properties of urban

Table 4 NDVI, NDBI and LST values for acquired images

Image acquisition date	NDVI			NDBI			LST		
	Max	Min	Mean	Max	Min	Mean	Max	Min	Mean
7 th April	0.49	-0.12	0.16	0.17	-0.36	-0.06	38.46	16.40	28.70
23 rd April	0.51	-0.16	0.14	0.20	-0.34	0.04	48.36	27.91	41.25

Table 5 Correlation between LST, NDVI and NDBI

	LST	NDVI	NDBI
LST	1	-	-
NDVI	-0.65895	1	-
NDBI	0.738143	-0.85835	1

and rural areas that ultimately affect thermal conditions by evaporation, heat storage, reflectance etc. (Gallo *et al.* 1993). A study by Gallo and Owen (1999) examined that the seasonal variations in LST and NDVI values accounts for 40% of differences in urban and surrounding rural temperatures. Also, the temperature of an area is directly linked with the amount of vegetation present there. The latent heat flux from the surface to atmosphere by vegetation determines the land surface temperature. The higher amount of vegetation in a pixel is depicted by higher NDVI value corresponding to low LST values.

3.4 NDBI

The built-up area of the district has been examined using NDBI index. The highest NDBI value for the study area is 0.17 with lowest NDBI value of -0.36 and an average of -0.06 for 7th April, 2018. The spatial pattern of NDBI for Mansa district calculated using Landsat 8 satellite data is displayed in Figs. 7(c) and 8(c). From the map, the dominance of built-up area can be observed for eastern part of the district. The dense built-up area of the district shows high NDBI values while negative values are observed for vegetated surfaces, water bodies distributed in the western part of the study area. The patches of settlements with high concentration of buildings have higher NDBI values than the open land.

For the second image, highest and lowest NDBI values are 0.20 and -0.34 respectively with an average of 0.04. The increased difference between average NDBI values of these two images is also due to the crop harvesting. The harvested agricultural fields resemble the open surface and hence are covered by built-up index. Also, the population in urban areas has expanded the built-up area, network of roads and other impervious surfaces with consequent loss of vegetation thereby leading to higher NDBI values of urban areas.

3.5 Correlation between LST and NDVI, NDBI

The significant influence of LULC indicators such as NDVI, NDWI and NDBI on LST has been documented in previous literature revealing that the relationship among these LULC indicators show temporal variations and also depict these indices as significant tools for quantitative analysis of surface temperature (Chen *et al.* 2006, Yuan and Bauer 2007, Liu and

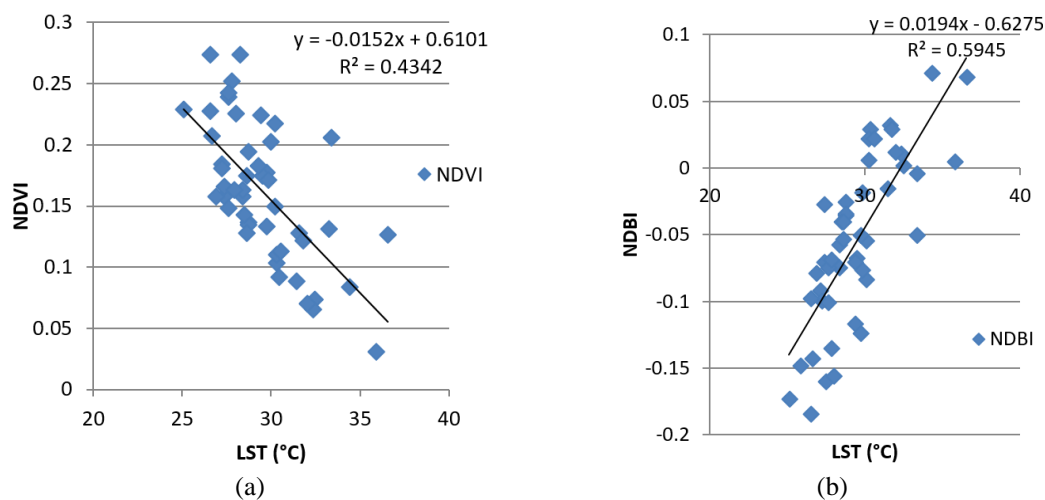


Fig. 9 Scatter plots for relationship among (a) LST and NDVI and (b) LST and NDBI

Zhang 2011). Therefore, the correlation study was carried out among LST and LULC parameters i.e., NDVI and NDBI, to examine the relationship between the LST and type of land cover for the study area. The temperature variations and distribution of vegetation and built-up surfaces has been observed for 48 sites by creating point features for the Mansa district. These temperature variations and indices values were then exported as XML file and used as input for Pearson correlation analysis.

So, the correlation examined for 48 observations of LST, NDVI and NDBI of the study area extracted using Landsat 8 satellite data is tabulated in Table 5:

Table 5 shows negative correlation between LST and NDVI with (correlation coefficient) $r = -0.659$ while positive correlation among NDBI and LST can be seen, with $r = 0.738$. Besides, negative correlation between NDVI and NDBI with $r = -0.858$, is also evident for the district. The statistical analysis carried out in this study illustrates similar results as observed for previous studies done by Santos *et al.* (2017) for Vila Velha, Brazil; Kikon *et al.* (2016) for Noida, India; Mallick *et al.* (2008) for Delhi, India; Liang and Weng (2008) for Indianapolis, US.

Furthermore, the Fig. 9 indicates the scatter plots depicting relationship between LST and NDVI, LST and NDBI.

The negative correlation between LST and NDVI is clearly evident from the scatter plot as low NDVI sites have higher LST value and vice-versa. The regression equation thus obtained for LST and NDVI is: $y = -0.015x + 0.610$ with the (coefficient of determination) $r^2 = 0.434$.

On the other side, regression equation $y = 0.019x - 0.627$, with the (coefficient of determination) $r^2 = 0.594$, has been obtained for NDBI and LST affirming a positive correlation among them. This positive correlation can be explained as the impervious built-up surfaces with less water storage capacity, lower down the humidity. This decreased humidity refers to less transpiration from land surface and ultimately rise of surface temperature (Lu *et al.* 2009, Santos *et al.* 2017). Additionally, high heat storage capacity of anthropogenic built-up surfaces made up of concrete, asphalt etc. with low albedo causes higher solar radiation absorption, which raises urban surface temperature.

The negative correlation analyzed among NDVI and LST validated in existing literature is due

Table 6 Comparison of LST extracted from Landsat satellite data air temperature

Site code	Minimum air temperature		Maximum air temperature		Mean air temperature		Land surface temperature	
	7 th April	23 rd April	7 th April	23 rd April	7 th April	23 rd April	7 th April	23 rd April
S1	25.1	23.6	35.8	33.4	30.45	28.5	32.24	41.09
S2	23.4	24.1	33.2	33.6	28.3	28.85	31.94	40.23
S3	23.8	25.5	32.2	34.5	28	30	31.43	42.01
S4	22.1	22.1	34.6	35.6	28.35	28.85	33.38	42.24
S5	19.9	21.8	33.7	32.5	26.8	27.15	31.01	40.69
S6	21.6	20.1	30.8	31.9	26.2	26	31.31	41.59

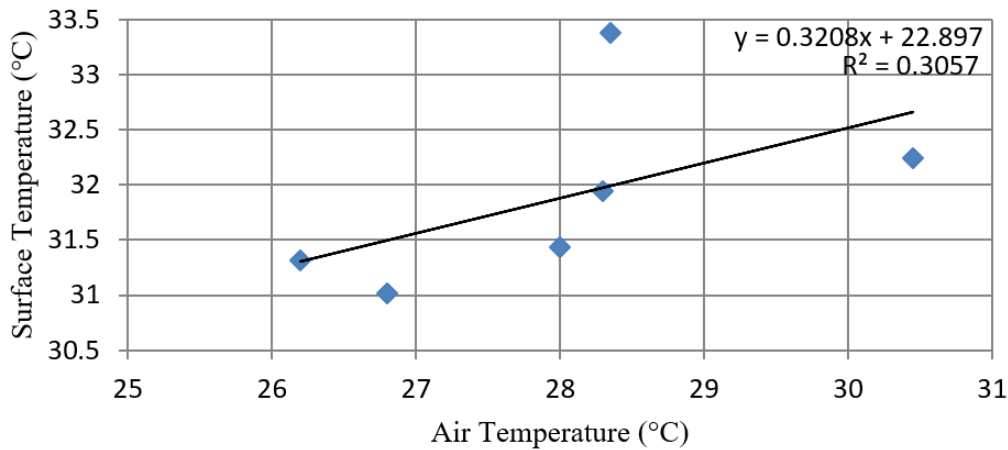


Fig. 10 Scatter plot for the comparison of LST with the air temperature for the study area

to the cooling effect of vegetation on the land surface temperature (Kumari *et al.* 2018). The vegetation absorbs the thermal energy and releases it as water vapor by transpiration, hence cooling the nearby air. Also, the trees provide shade preventing direct heating of surface by incoming solar radiations, thus preventing rise in temperature (Senanayake *et al.* 2013). So, the negative correlation between NDVI and LST is significant for urban climate studies and hence, the major reason for which vegetation is considered as an important mitigation measure of UHI effect, cited in many research studies.

3.6 Comparison between LST and in-situ observations

The satellite data facilitates higher spatial area coverage whereas higher temporal resolution can be obtained from in-situ observations. So, the use of both satellite and in-situ observations provides more information regarding UHI effect for the study area. Furthermore, the statistical analysis of both the observations depicts the relationship among them as there are various surface energy balance processes that strongly relate both the surface and air temperatures together. The air temperature of lower layers of the atmosphere is modulated by the land surface temperature of that region (Voogt and Oke 2003). Thus, this study compares both the air temperature recorded

using field observations and LST retrieved using satellite data (shown in Table 6) for higher knowledge regarding UHI effect. The LST derived from satellite data is taken for same geographical co-ordinates that of air temperature measured using Mextech digital thermometers.

Positive correlation ($r= 0.553$) is analyzed between air and surface temperature (Fig. 10). The air temperature recorded as few meters above the ground level shows higher variations than that of surface temperature for six sites of Mansa district of Punjab. The surface temperature values are high due to complex urban surfaces and different types of urban topography (Nichol 1996, Streutker 2002). The surface UHI thus differs from atmospheric UHI due to temperature variations in air and land surface because of variations in heat capacities of air and land surface. Moreover, strong correlation between LST derived from remote sensing data and temperature from field observations has been validated in earlier UHI studies conducted by Fung *et al.* (2009) for and Klok *et al.* (2012) for Rotterdam, Netherlands concluding that the variations in spatial pattern of Hong Kong surface temperature represents air temperature variations. Also, Chakraborty *et al.* (2015) carried out a comparison study between LST derived from Landsat satellite data and from ground measurements using thermal infrared thermometers, and determined a close correlation between both the temperatures. The comparison study for in-situ observations and remote sensing observations carried out by Mohan *et al.* (2012) in Delhi showed that UHI hotspots were well correlated for nighttime only.

4. Conclusions

The rising population has significantly developed urban areas by changing LULC patterns. The continuing transformation of rural vegetated areas into built-up areas at noticeable rate has significant influence on urban climate implying UHI effect. The introduction of remote sensing and GIS technology has brought new insights in this field for better quantification of UHI effect. So, this study involves the use of satellite remote sensing for monitoring spatial distribution of LST because of its time saving procedure and cost-effectiveness. This paper presents a case study for an urban area of Punjab having following main aspects i.e., investigation of LST retrieved using TIR band of Landsat 8 comparing UHI occurrence of remote sensing data and field observations. The significant temperature variations were observed for the study area. The results of diurnal variations of air temperature for the study area depicted higher UHI effect during night hours for urban sites. The LST retrieved from Landsat 8 data was observed higher for the urban clusters with dense infrastructure due to lack of vegetation content and water surfaces. The NDVI, NDBI depicting the land use pattern of area were analyzed to evaluate the impact of LULC on UHI effect. The study concludes in finding negative correlation between NDVI and LST due to cooling effect of vegetation on the land surface temperature whereas NDBI and LST are positively correlated with each other. The air and land surface temperature were found to have positive correlation by Pearson correlation analysis. So, this study facilitates the warm pockets of Mansa district that can be helpful in proper planning of urbanization to maintain the thermal comfort of city residents. It also demonstrates the need of green cover in urban areas.

References

- Adams, M.P. and Smith, P.L. (2014), "A systematic approach to model the influence of the type and density of vegetation cover on urban heat using remote sensing", *Landsc. Urban Plan.*, **132**, 47-54.

- <https://doi.org/10.1016/j.landurbplan.2014.08.008>.
- Alonso, M.S., Labajo, J.L. and Fidalgo, M.R. (2003), "Characteristics of the urban heat island in the city of Salamanca, Spain", *Atmosfera*, **16**(3), 137-148.
- Artis, D.A. and Carnahan, W.H. (1982), "Survey of emissivity variability in thermography of urban areas", *Remote Sens. Environ.*, **12**(4), 313-329. [https://doi.org/10.1016/0034-4257\(82\)90043-8](https://doi.org/10.1016/0034-4257(82)90043-8).
- Azevedo, J., Chapman, L. and Muller, C. (2016), "Quantifying the daytime and night-time urban heat island in Birmingham, UK: A comparison of satellite derived land surface temperature and high resolution air temperature observations", *Remote Sensing*, **8**(2), 153. <https://doi.org/10.3390/rs8020153>.
- Borbora, J. and Das A.K. (2014), "Summertime urban heat island study for Guwahati city, India", *Sustain. Cities Soc.*, **11**, 61-66. <https://doi.org/10.1016/j.scs.2013.12.001>.
- Chakraborty, S.D., Kant, Y. and Mitra, D. (2015), "Assessment of land surface temperature and heat fluxes over Delhi using remote sensing data", *J. Environ. Manage.*, **148**, 143-152. <https://doi.org/10.1016/j.jenvman.2013.11.034>.
- Chen, X.L., Zhao, H.M., Li, P.X. and Yin, Z.Y. (2006), "Remote sensing image-based analysis of the relationship between urban heat island and land use/cover changes", *Remote Sens. Environ.*, **104**(2), 133-146. <https://doi.org/10.1016/j.rse.2005.11.016>.
- Cheng, C., Cai, Z., Yan, W., Li, H.Y., Meng, W.Q., Hao, C. and Mo, X.Q. (2010), "Study of temporal and spatial variation of urban heat island based on Landsat TM in central city and binhai new area of Tianjin", *J. Nat. Resour.*, **25**(10), 1727-1737.
- dos Santos, A.R., de Oliveira, F.S., da Silva, A.G., Gleriani, J.M., Gonçalves, W., Moreira, G.L., Silva, F.G., Branco, E.R.F., Moura, M.M., da Silva, R.G. and Juvanhol, R.S. (2017), "Spatial and temporal distribution of urban heat islands", *Sci. Total Environ.*, **605-606**, 946-956. <http://dx.doi.org/10.1016/j.scitotenv.2017.05.275>.
- Eliasson, I. (1994), "Urban-suburban-rural air temperature differences related to street geometry", *Phys. Geograph.*, **15**(1), 1-22. <https://doi.org/10.1080/02723646.1994.10642501>
- EPA (2009), Heat Island Effect, <http://www.epa.gov/heatisland/about/index.htm>.
- Farina, A. (2012), "Exploring the relationship between land surface temperature and vegetation abundance for urban heat island mitigation in Seville, Spain", LUMA-GIS Thesis.
- Fung, W.Y., Lam, K.S., Nichol, J. and Wong, M.S. (2009), "Derivation of nighttime urban air temperatures using a satellite thermal image", *J. Appl. Meteorol. Clim.*, **48**(4), 863-872. <https://doi.org/10.1175/2008JAMC2001.1>.
- Gallo, K.P. and Owen, T.W. (1999), "Satellite-based adjustments for the urban heat island temperature bias", *J. Appl. Meteorol.*, **38**(6), 806-813. [https://doi.org/10.1175/1520-0450\(1999\)038<0806:SBAFTU>2.0.CO;2](https://doi.org/10.1175/1520-0450(1999)038<0806:SBAFTU>2.0.CO;2)
- Gallo, K.P., McNab, A.L., Karl, T.R., Brown, J.F., Hood, J.J. and Tarpley, J.D. (1993), "The use of a vegetation index for assessment of the urban heat island effect", *Remote Sens.*, **14**(11), 2223-2230. <https://doi.org/10.1080/01431169308954031>
- Gedzelman, S.D., Austin, S., Cermak, R., Stefano, N., Partridge, S., Quesenberry, S. and Robinson, D.A. (2003), "Mesoscale aspects of the urban heat island around New York City", *Theor. Appl. Climatol.*, **75**(1), 29-42. <https://doi.org/10.1007/s00704-002-0724-2>.
- Giridharan, R., Ganesan, S. and Lau, S.S.Y. (2004), "Daytime urban heat island effect in high-rise and high-density residential developments in Hong Kong", *Energy Build.*, **36**(6), 525-534. <https://doi.org/10.1016/j.enbuild.2003.12.016>.
- Gober, P., Brazel, A., Quay, R., Myint, S., Grossman-Clarke, S., Miller, A. and Rossi, S. (2009), "Using watered landscapes to manipulate urban heat island effects: how much water will it take to cool Phoenix?", *J. Amer. Plan. Assoc.*, **76**(1), 109-121. <https://doi.org/10.1080/01944360903433113>.
- Grimm, N.B., Faeth, S.H., Golubiewski, N.E., Redman, C.L., Wu, J., Bai, X. and Briggs, J.M. (2008), "Global change and the ecology of cities", *Science*, **319**(5864), 756-760. <https://doi.org/10.1126/science.1150195>.
- Habert, G. and Schlueter, A. (2016), *Expanding Boundaries: Systems Thinking in the Built Environment: Sustainable Built Environment (SBE) Regional Conference Zurich 2016*. vdfHochschulverlag AG.

- Han, S., Bian, H., Tie, X., Xie, Y., Sun, M. and Liu, A. (2009), "Impact of nocturnal planetary boundary layer on urban air pollutants: Measurements from a 250-m tower over Tianjin, China", *J. Hazard. Mater.*, **162**(1), 264-269. <https://doi.org/10.1016/j.jhazmat.2008.05.056>.
- Imhoff, M.L., Zhang, P., Wolfe, R.E. and Bounoua, L. (2010), "Remote sensing of the urban heat island effect across biomes in the continental USA", *Remote Sens. Environ.*, **114**(3), 504-513. <https://doi.org/10.1016/j.rse.2009.10.008>.
- Julien, Y., Sobrino, J.A., Mattar, C., Ruescas, A.B., Jimenez-Munoz, J.C., Soria, G., Hidalgo, V., Atitar, M., Franch, B. and Cuenca, J. (2011), "Temporal analysis of normalized difference vegetation index (NDVI) and land surface temperature (LST) parameters to detect changes in the Iberian land cover between 1981 and 2001", *Int. J. Remote Sens.*, **32**(7), 2057-2068. <https://doi.org/10.1080/01431161003762363>.
- Karl, T.R., Diaz, H.F. and Kukla, G. (1988), "Urbanization: Its detection and effect in the United States climate record", *J. Climate*, **1**(11), 1099-1123. [https://doi.org/10.1175/1520-0442\(1988\)001<1099:UIDAEI>2.0.CO;2](https://doi.org/10.1175/1520-0442(1988)001<1099:UIDAEI>2.0.CO;2)
- Kikon, N., Singh, P., Singh, S.K. and Vyas, A. (2016), "Assessment of urban heat islands (UHI) of Noida City, India using multi-temporal satellite data", *Sustain. Cities Soc.*, **22**, 19-28. <https://doi.org/10.1016/j.scs.2016.01.005>.
- Kim, Y.H. and Baik, J.J. (2004), "Daily maximum urban heat island intensity in large cities of Korea", *Theor. Appl. Climatol.*, **79**(3-4), 151-164. <https://doi.org/10.1007/s00704-004-0070-7>.
- Kim, Y.H. and Baik, J.J. (2005), "Spatial and temporal structure of the urban heat island in Seoul", *J. Appl. Meteorol.*, **44**, 591-605. <https://doi.org/10.1175/JAM2226.1>.
- Klok, L., Zwart, S., Verhagen, H. and Mauri, E. (2012), "The surface heat island of Rotterdam and its relationship with urban surface characteristics", *Resour. Conserv. Recycling*, **64**, 23-29. <https://doi.org/10.1016/j.resconrec.2012.01.009>.
- Kolokotroni, M. and Giridharan, R. (2008), "Urban heat island intensity in London: An investigation of the impact of physical characteristics on changes in outdoor air temperature during summer", *Solar Energy*, **82**(11), 986-998. <https://doi.org/10.1016/j.solener.2008.05.004>.
- Kovats, R.S. and Hajat, S. (2008), "Heat stress and public health: a critical review", *Ann. Rev. Public Health*, **29**, 41-55. <https://doi.org/10.1146/annurev.publhealth.29.020907.090843>.
- Kuang, W., Liu, Y., Dou, Y., Chi, W., Chen, G., Gao, C., Yang, T., Liu, J. and Zhang, R. (2015), "What are hot and what are not in an urban landscape: Quantifying and explaining the land surface temperature pattern in Beijing, China", *Landscape Ecol.*, **30**(2), 357-373. <https://doi.org/10.1007/s10980-014-0128-6>.
- Kumari, B., Tayyab, M., Mallick, J., Khan, M.F. and Rahman, A. (2018), "Satellite-driven land surface temperature (LST) using Landsat 5, 7 (TM/ETM+ SLC) and Landsat 8 (OLI/TIRS) data and its association with built-up and green cover over urban Delhi, India", *Remote Sen. Earth Syst. Sci.*, **1**(3-4), 63-78. <https://doi.org/10.1007/s41976-018-0004-2>.
- Lam, K.S., Wang, T.J., Wu, C.L. and Li, Y.S. (2005), "Study on an ozone episode in hot season in Hong Kong and transboundary air pollution over Pearl River Delta region of China", *Atmosph. Environ.*, **39**(11), 1967-1977. <https://doi.org/10.1016/j.atmosenv.2004.11.023>.
- Landsberg, H.E. (1981), *The Urban Climate (Vol. 28)*, Academic Press.
- Lemonsu, A., Viguie, V., Daniel, M. and Masson, V. (2015), "Vulnerability to heat waves: Impact of urban expansion scenarios on urban heat island and heat stress in Paris (France)", *Urban Climate*, **14**, 586-605. <https://doi.org/10.1016/j.uclim.2015.10.007>.
- Li, W., Bai, Y., Chen, Q., He, K., Ji, X. and Han, C. (2014), "Discrepant impacts of land use and land cover on urban heat islands: A case study of Shanghai, China", *Ecol. Indicators*, **47**, 171-178. <https://doi.org/10.1016/j.ecolind.2014.08.015>.
- Liang, B. and Weng, Q. (2008), "Multiscale analysis of census-based land surface temperature variations and determinants in Indianapolis, United States", *J. Urban Plan. Dev.*, **134**(3), 129-139. [https://doi.org/10.1061/\(ASCE\)0733-9488\(2008\)134:3\(129\)](https://doi.org/10.1061/(ASCE)0733-9488(2008)134:3(129)).
- Liu, L. and Zhang, Y. (2011), "Urban heat island analysis using the Landsat TM data and ASTER data: A case study in Hong Kong", *Remote Sens.*, **3**(7), 1535-1552. <http://dx.doi.org/10.3390/rs3071535>.
- Lo, C.P. and Quattrochi, D.A. (2003), "Land-use and land-cover change, urban heat island phenomenon, and

- health implications”, *Photogram. Eng. Remote Sens.*, **69**(9), 1053-1063. <https://doi.org/10.14358/PERS.69.9.1053>.
- Lu, Y., Feng, P., Shen, C. and Sun, J. (2009), “Urban heat island in summer of Nanjing based on TM data”, *Proceedings of the 2009 Joint Urban Remote Sensing Event*, Shanghai, China, May.
- Mallick, J. (2014), “Land characterization analysis of surface temperature of semi-arid mountainous city Abha, Saudi Arabia using remote sensing and GIS”, *J. Geograph. Inform. Syst.*, **6**(06), 664. <https://doi.org/10.4236/jgis.2014.66055>.
- Mallick, J., Kant, Y. and Bharath, B.D. (2008), “Estimation of land surface temperature over Delhi using Landsat-7 ETM+”, *J. Ind. Geophys. Union*, **12**(3), 131-140.
- Markham, B.L., Storey, J.C., Williams, D.L. and Irons, J.R. (2004), “Landsat sensor performance: history and current status”, *IEEE T. Geosci. Remote Sens.*, **42**(12), 2691-2694. <https://doi.org/10.1109/TGRS.2004.840720>.
- Mathew, A., Khandelwal, S. and Kaul, N. (2016), “Spatial and temporal variations of urban heat island effect and the effect of percentage impervious surface area and elevation on land surface temperature: Study of Chandigarh city, India”, *Sustain. Cities Soc.*, **26**, 264-277. <https://doi.org/10.1016/j.scs.2016.06.018>.
- Mathew, A., Khandelwal, S. and Kaul, N. (2018), “Analysis of diurnal surface temperature variations for the assessment of surface urban heat island effect over Indian cities”, *Energy Build.*, **159**, 271-295. <https://doi.org/10.1016/j.enbuild.2017.10.062>
- Mohan, M., Kikegawa, Y., Gurjar, B.R., Bhati, S., Kandya, A. and Ogawa, K. (2012), “Urban heat island assessment for a tropical urban airshed in India”, *Atmosph. Climate Sci.*, **2**(2), 127-138. <https://doi.org/10.4236/acs.2012.22014>.
- Mukherjee, S., Joshi, P.K. and Garg, R.D. (2017), “Analysis of urban built-up areas and surface urban heat island using downscaled MODIS derived land surface temperature data”, *Geocarto Int.*, **32**(8), 900-918. <https://doi.org/10.1080/10106049.2016.1222634>.
- Nesarikar-Patki, P. and Raykar-Alange, P. (2012), “Study of influence of land cover on urban heat islands in pune using remote”, *IOSR J. Mech. Civ. Eng.*, **3**, 39-43.
- Nichol, J.E. (1996), “High-resolution surface temperature patterns related to urban morphology in a tropical city: A satellite-based study”, *J. Appl. Meteorol.*, **35**(1), 135-146. [https://doi.org/10.1175/1520-0450\(1996\)035<0135:HRSTPR>2.0.CO;2](https://doi.org/10.1175/1520-0450(1996)035<0135:HRSTPR>2.0.CO;2).
- Oke, T.R. (1981), “Canyon geometry and the nocturnal urban heat island: comparison of scale model and field observations”, *J. Climatol.*, **1**(3), 237-254. <https://doi.org/10.1002/joc.3370010304>.
- Oke, T.R. (1982), “The energetic basis of the urban heat island”, *Quart. J. Royal Meteorol. Soc.*, **108**(455), 1-24. <https://doi.org/10.1002/qj.49710845502>.
- Oke, T.R. (1987), *Boundary Layer Climate*, 2nd Edition. Routledge, 435.
- Pandey, A.K., Singh, S., Berwal, S., Kumar, D., Pandey, P., Prakash, A., Lodhi, N., Maithani, S., Jain, V.K. and Kumar, K. (2014), “Spatio-temporal variations of urban heat island over Delhi”, *Urban Climate*, **10**, 119-133. <https://doi.org/10.1016/j.uclim.2014.10.005>.
- Pandey, P., Kumar, D., Prakash, A., Masih, J., Singh, M., Kumar, S., Jain, V.K. and Kumar, K. (2012), “A study of urban heat island and its association with particulate matter during winter months over Delhi”, *Sci. Total Environ.*, **414**, 494-507. <https://doi.org/10.1016/j.scitotenv.2011.10.043>.
- PCA (2011), *Primary Census Abstract*, in *District Census Handbook Mansa*, Series-04, PART XII-B, Census of India 2011, Punjab, India.
- Phiri, D. and Morgenroth, J. (2017), “Developments in Landsat land cover classification methods: A review”, *Remote Sens.*, **9**(9), 967. <https://doi.org/10.3390/rs9090967>.
- Rajasekar, U. and Weng, Q. (2009), “Spatio-temporal modelling and analysis of urban heat islands by using Landsat TM and ETM+ imagery”, *Int. J. Remote Sens.*, **30**(13), 3531-3548. <https://doi.org/10.1080/01431160802562289>.
- Rajeshwari, A. and Mani, N.D. (2014), “Estimation of land surface temperature of Dindigul district using Landsat 8 data”, *Int. J. Res. Eng. Technol.*, **3**(5), 122-126.
- Roth, M., Oke, T.R. and Emery, W.J. (1989), “Satellite-derived urban heat islands from three coastal cities

- and the utilization of such data in urban climatology”, *Int. J. Remote Sens.*, **10**(11), 1699-1720. <https://doi.org/10.1080/01431168908904002>.
- Santamouris, M. (2015), “Regulating the damaged thermostat of the cities—Status, impacts and mitigation challenges”, *Energy Build.*, **91**, 43-56. <https://doi.org/10.1016/j.enbuild.2015.01.027>.
- Sarrat, C., Lemonsu, A., Masson, V. and Guedalia, D. (2006), “Impact of urban heat island on regional atmospheric pollution”, *Atmosph. Environ.*, **40**(10), 1743-1758. <https://doi.org/10.1016/j.atmosenv.2005.11.037>.
- Senanayake, I.P., Welivitiya, W.D.D.P. and Nadeeka, P.M. (2013), “Remote sensing based analysis of urban heat islands with vegetation cover in Colombo city, Sri Lanka using Landsat-7 ETM+ data”, *Urban Climate*, **5**, 19-35. <http://dx.doi.org/10.1016/j.uclim.2013.07.004>.
- Shastri, H., Barik, B., Ghosh, S., Venkataraman, C. and Sadavarte, P. (2017), “Flip flop of day-night and summer-winter surface urban heat island intensity in India”, *Sci. Reports*, **7**(1), 40178. <https://doi.org/10.1038/srep40178>.
- Shastri, H., Paul, S., Ghosh, S. and Karmakar, S. (2015), “Impacts of urbanization on Indian summer monsoon rainfall extremes”, *J. Geophys. Res. Atmosph.*, **120**(2), 496-516. <https://doi.org/10.1002/2014JD022061>.
- Singh, R., Grover, A. and Zhan, J. (2014), “Inter-seasonal variations of surface temperature in the urbanized environment of Delhi using Landsat thermal data”, *Energies*, **7**(3), 1811-1828. <https://doi.org/10.3390/en7031811>.
- Sobrino, J.A., Jimenez-Munoz, J.C. and Paolini, L. (2004), “Land surface temperature retrieval from Landsat TM 5”, *Remote Sens. Environ.*, **90**, 434-440. <https://doi.org/10.1016/j.rse.2004.02.003>.
- Stathopoulou, M., Cartalis, C. and Petrakis, M. (2007), “Integrating Corine Land Cover data and Landsat TM for surface emissivity definition: application to the urban area of Athens, Greece”, *Int. J. Remote Sens.*, **28**(15), 3291-3304. <https://doi.org/10.1080/01431160600993421>.
- Steenveld, G.J., Koopmans, S., Heusinkveld, B.G., Van Hove, L.W.A. and Holtslag, A.A.M. (2011), “Quantifying urban heat island effects and human comfort for cities of variable size and urban morphology in the Netherlands”, *J. Geophys. Res. Atmosph.*, **116**(D20). <https://doi.org/10.1029/2011JD015988>.
- Stewart, I.D. (2011), “A systematic review and scientific critique of methodology in modern urban heat island literature”, *Int. J. Climatol.*, **31**(2), 200-217. <https://doi.org/10.1002/joc.2141>.
- Streutker, D.R. (2002), “A remote sensing study of the urban heat island of Houston, Texas”, *Int. J. Remote Sens.*, **23**(13), 2595-2608. <http://dx.doi.org/10.1080/01431160110115023>.
- Sun, Q., Tan, J. and Xu, Y. (2010), “An ERDAS image processing method for retrieving LST and describing urban heat evolution: a case study in the Pearl River Delta Region in South China”, *Environ. Earth Sci.*, **59**(5), 1047-1055. <https://doi.org/10.1007/s12665-009-0096-3>.
- Svensson, M.K. (2004), “Sky view factor analysis-implications for urban air temperature differences”, *Meteorol. Appl.*, **11**(3), 201-211. <https://doi.org/10.1017/S1350482704001288>.
- Taha, H. (1997), “Urban climates and heat islands: albedo, evapotranspiration, and anthropogenic heat”, *Energy Build.*, **25**(2), 99-103. [https://doi.org/10.1016/S0378-7788\(96\)00999-1](https://doi.org/10.1016/S0378-7788(96)00999-1).
- Vitousek, P.M., Mooney, H.A., Lubchenco, J. and Melillo, J.M. (1997), “Human domination of Earth’s ecosystems”, *Science*, **277**(5325), 494-499. <https://doi.org/10.1126/science.277.5325.494>.
- Voogt, J.A. and Oke, T.R. (1998), “Effects of urban surface geometry on remotely-sensed surface temperature”, *Int. J. Remote Sens.*, **19**(5), 895-920. <https://doi.org/10.1080/014311698215784>.
- Yadav, N., Sharma, C., Peshin, S.K. and Masiwal, R. (2017), “Study of intra-city urban heat island intensity and its influence on atmospheric chemistry and energy consumption in Delhi”, *Sustain. Cities Soc.*, **32**, 202-211. <https://doi.org/10.1016/j.scs.2017.04.003>.
- Yuan, F. and Bauer, M.E. (2007), “Comparison of impervious surface area and normalized difference vegetation index as indicators of surface urban heat island effects in Landsat imagery”, *Remote Sens. Environ.*, **106**(3), 375-386. <https://doi.org/10.1016/j.rse.2006.09.003>.
- Zha, Y., Gao, J. and Nil, S. (2003), “Use of normalized difference built-up index in automatically mapping urban areas from TM imagery”, *Int. J. Remote Sens.*, **24**(3), 583-594.

<http://dx.doi.org/10.1080/01431160304987>.

Zhang, H., Qi, Z.F., Ye, X.Y., Cai, Y.B., Ma, W.C. and Chen, M.N. (2013), "Analysis of land use/land cover change, population shift, and their effects on spatiotemporal patterns of urban heat islands in metropolitan Shanghai, China", *Appl. Geograph.*, **44**, 121-133.
<https://doi.org/10.1016/j.apgeog.2013.07.021>.

CC